AD-A190 136 EXPERIMENTAL INVESTIGATION OF A SPANWISE FORCED MIXING LAYER(U) ARIZONA UNIV TUCSON A GLEZER ET AL 07 NOV 87 AFOSR-TR-87-1903 AFOSR-86-0324 1/1

UNCLASSIFIED F/G 20/4 NL

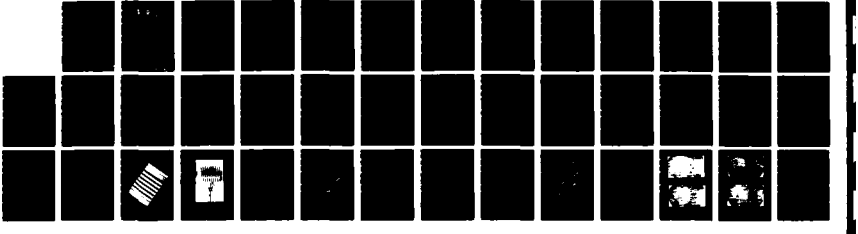

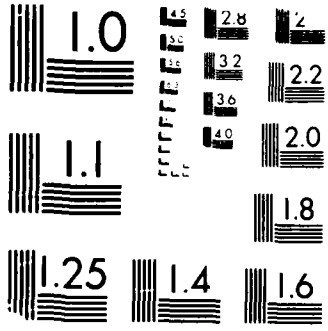

UNCLASSIFIED

SECURITY CLASSIFICATION OF THIS PAGE

REPORT DOCUMENTATION PAGE

1a. REPORT SECURITY CLASSIFICATION: UNCLASSIFIED	1b. RESTRICTIVE MARKINGS
2a. SECURITY CLASSIFICATION AUTHORITY	3. DISTRIBUTION/AVAILABILITY OF REPORT: APPROVED FOR PUBLIC RELEASE DISTRIBUTION IS UNLIMITED
2b. DECLASSIFICATION/DOWNGRADING SCHEDULE	
4. PERFORMING ORGANIZATION REPORT NUMBER(S)	5. MONITORING ORGANIZATION REPORT NUMBER(S): AFOSR-TR- 87-1903
6a. NAME OF PERFORMING ORGANIZATION: University of Arizona; 6b. OFFICE SYMBOL (If applicable)	7a. NAME OF MONITORING ORGANIZATION: AFOSR/NA
6c. ADDRESS (City, State and ZIP Code): Tucson, Arizona 85721	7b. ADDRESS (City, State and ZIP Code): BUILDING 410, BOLLING AFB, DC 20332-6448
8a. NAME OF FUNDING/SPONSORING ORGANIZATION: AFOSR/NA; 8b. OFFICE SYMBOL (If applicable): NA	9. PROCUREMENT INSTRUMENT IDENTIFICATION NUMBER: AFOSR-86-0324
8c. ADDRESS (City, State and ZIP Code): BUILDING 410, BOLLING AFB, DC 20332-6448	10. SOURCE OF FUNDING NOS: PROGRAM ELEMENT NO 61102F; PROJECT NO. 2307; TASK NO. A2; WORK UNIT NO.
11. TITLE (Include Security Classification): Experimental Investigation of a Spanwise Forced Mixing Layer	
12. PERSONAL AUTHOR(S): A. Glezer, I.J. Wygnanski, T.F. Balsa	
13a. TYPE OF REPORT: Annual; 13b. TIME COVERED: FROM 7/1/86 TO 6/30/87	14. DATE OF REPORT (Yr., Mo., Day): 1987 Nov 7; 15. PAGE COUNT: 39
16. SUPPLEMENTARY NOTATION	
17. COSATI CODES: FIELD / GROUP / SUB GR	18. SUBJECT TERMS (Continue on reverse if necessary and identify by block number): Mixing Layer, Spanwise Forcing, Coherent Structures, Hotwires, Schlieren ←

19. ABSTRACT (Continue on reverse if necessary and identify by block number)

The occurrence of three-dimensional motion within a plane mixing layer results in a significant increase of the internal mixedness (mixing transition). The three-dimensional motion necessary for mixing is induced by streamwise, counter-rotating vortex pairs superimposed on the primary spanwise vortices. While their appearance in the plane mixing layer has been established, their origin and their evolution with increasing streamwise distance remains an enigma. Stability considerations indicate that an instability in the spanwise direction may lead to the generation of streamwise vorticity. This suggests that the flow may be susceptible to low level spanwise periodic forcing. Previous experiments have demonstrated that forcing allows the enhancement of individual instability modes and is an essential step towards understanding the evolution of the natural flow. Furthermore, application of forcing to the flow provides a powerful tool of considerable practical significance for the control of the downstream evolution.

We have begun an experimental investigation of a plane mixing layer which is forced independently in the spanwise and streamwise directions. Our objective is to study the evolution of spanwise instability, its role in the development of the plane mixing layer and possible interaction between the streamwise and spanwise instabilities. Forcing is applied by a spanwise line of discrete surface film heaters flush mounted on the flow partition. This technique enables us to study nonlinear interactions between various modes of spanwise and streamwise instabilities.

20. DISTRIBUTION/AVAILABILITY OF ABSTRACT: UNCLASSIFIED/UNLIMITED ☒ SAME AS RPT ☐ DTIC USERS ☐	21. ABSTRACT SECURITY CLASSIFICATION: UNCLASSIFIED
22a. NAME OF RESPONSIBLE INDIVIDUAL: JAMES M MCMICHAEL	22b. TELEPHONE NUMBER (Include Area Code): 202-767-4935; 22c. OFFICE SYMBOL: AFOSR/NA

DD FORM 1473, 83 APR — EDITION OF 1 JAN 73 IS OBSOLETE

UNCLASSIFIED

Research Progress and Forecast Report

EXPERIMENTAL INVESTIGATION OF A SPANWISE FORCED MIXING LAYER

Grant No. AFOSR-86-0324

Period Covered 7/1/86 - 6/30/87

Submitted to

Air Force Office of Scientific Research
Bolling Air Force Base, Building 410
Washington, D.C. 20332

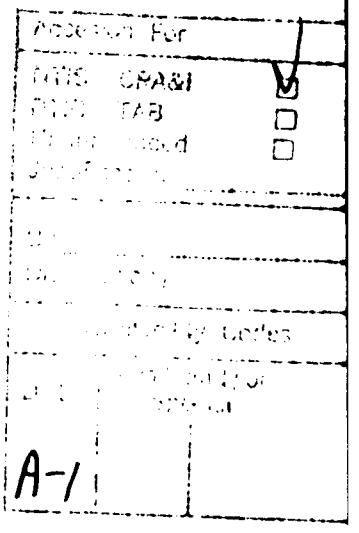

Submitted by

A. Glezer, I.J. Wygnanski, T.F. Balsa
Department of Aerospace and Mechanical Engineering
University of Arizona
Tucson, Arizona 85721

Experimental and Analytical Investigation of a Spanwise Forced Mixing Layer

1. Brief Overview

The occurrence of three-dimensional motion within a plane mixing layer results in a significant increase of internal mixedness (Roshko 1980, Lin and Corcos 1984). The three-dimensional motion necessary for mixing is induced by streamwise, counter-rotating vortex pairs which are part of a vortex that continuously loops back and forth between adjacent spanwise vortices (Bernal and Roshko 1986, Lasheras, Choi and Maxworthy 1986). Stability studies (e.g., Pierrehumbert and Widnall 1982) as well as numerical calculations (Ashurst and Meiburg 1985, Metcalfe et al., 1986) indicate that an instability in the spanwise direction may lead to the generation of streamwise vorticity. These findings suggest (as confirmed by recent experiments of Lasheras and Choi 1987) that the flow may be susceptible to low level spanwise forcing. Previous experiments (Oster and Wygnanski 1982, Roberts and Roshko 1985) have demonstrated that streamwise forcing allows the enhancement of individual instability modes and hence is an essential step towards the understanding of the natural flow. Furthermore, these experiments show that streamwise forcing may significantly enhance or reduce the natural mixing between the two streams; they therefore suggest a possible interaction between the streamwise and spanwise instability modes. Given that many turbulent reacting flows of engineering interest involve turbulent shear layers, the application of forcing provides a powerful tool of considerable practical significance for understanding the flow structure and modifying its downstream evolution.

We have begun an experimental investigation of a plane mixing layer which is forced independently in the spanwise and streamwise directions. Our objective is to study the evolution of spanwise instability, its role in the development of the mixing layer, and possible interaction between the streamwise and spanwise instabilities. Forcing is applied by a mosaic of surface film heaters flush-mounted on the flow partition.

In the next section, we discuss the schedule for the second year of this work. The third section describes the development of our experimental methods and facilities, the extensive testing

and calibration of the experimental hardware, and preliminary results focusing on some new aspects of the forced mixing layer.

2. Schedule (July 1, 1987 - June 30, 1988)

Our research program focuses on the experimental and analytical investigation of a plane mixing layer which is forced independently in the spanwise and streamwise directions. Our objective is to study the evolution of the spanwise instabilities, their role in the development of the mixing layer and the possible interacions which might occur between the streamwise and spanwise instabilities. Forcing is applied by a mosaic of surface film heaters flush mounted on the partition separating the two streams. Detailed simultaneous spanwise measurements of the streamwise velocity will be conducted with a rake of hot wire probes. This work will be complemented with an analytical (theoretical/numerical) study of the weakly nonlinear interactions between streamwise and spanwise instabilities.

Given the spanwise array of heaters, the shear layer will be forced in the following time and space dependent configurations:

Consider a general surface temperature distribution

$$T(z,t) = T(z,t;\beta,\omega,T_0)$$

denoting

z = spanwise coordinate

β = spanwise wave number

ω = forcing frequency

T = forcing amplitude

(β,ω,and T_0 are programmable.)

The following forms of surface temperature distributions will be synthesized by the spanwise array of heaters.

(a) Steady spanwise-periodic forcing

$$T(z,t) = T[1 + \sin(\beta z)]$$

Steady heating induces regular spanwise velocity variations in the splitter plate boundary layers. Such forcing will circumvent the tendency of the spanwise instability to lock on to small (steady) disturbances within the experimental apparatus. We plan to study the effect of β on the downstream wavelength of the spanwise instability. Coupling between the (forced) spanwise mode and any streamwise mode will be investigated. This form of forcing has not been investigated theoretically or numerically. It is hoped that the results of this study will reveal interesting phenomena hitherto unknown.

(b) Travelling waves in the spanwise direction (spanwise phase modulated forcing)

$$T(z,t) = T[1 + \sin(\beta z - \omega t)]$$

An oblique travelling wave is produced. We intend to check the prediction of linear stability theory as applied to this nearly parallel flow using Squire's transformation.

(c) Standing waves in the spanwise direction (spanwise phase modulated forcing)

$$T(z,t) = T[1 + \cos(\omega t) \sin(\beta z + \phi)]$$

This is streamwise forcing with temporally steady spanwise variations. The structure of the secondary (streamwise) vortices will be investigated within the "frequency locked" region where the primary (spanwise) vortices are equally spaced and phase locked to the forcing frequency. The validity of Bernal and Roshko (1986) conjecture on the structure of the secondary vortex will be

established by phase averaged flow field measurements and flow visualization. We will also compare the two classes of instabilities discussed by Pierrehumbert and Widnall (1982) to our experimental results.

(d) Spanwise wavelength modulation

$$T(z,t) = T[1 + \sin(\beta z)]$$

where $\beta = \beta'[1 + \epsilon\cos\omega t]$.

Periodic variation of β at a fixed streamwise wave number α will be investigated to examine the nonlinear interactions between the streamwise and spanwise vortices. These measurements will be compared with the weakly nonlinear theory of Prof. T.F. Balsa describing the interactions between streamwise and spanwise modes.

During the summer of 1988, we plan to conduct similar experiments in the new Air Shear Layer Facility at the NASA Ames Fluid Mechanics Laboratory. This high aspect ratio facility will enable us to extend our investigations of spanwise structures to an environment which is virtually free of sidewall interference. We expect to collaborate on this research with Dr. R.D. Mehta of NASA Ames (including the development of a suitable forcing method for the air facility within the next year). During these experiments, we hope to use our ten-channel hot-wire anemometer and specially designed rakes of hot-wire probes. This instrumentation will be easily incorporated into the existing experimental apparatus due to the flexibility of the data acquisition system at the NASA Ames Fluid Mechanics Laboratory. The experimental program will be coordinated with Drs. S. Davis and R.D. Mehta during the next year.

In addition to the conventional velocity measurements, we expect to introduce a novel technique which utilizes the streaks of neutrally buoyant phosphorescent particles uniformly distributed in the flow. These data will be analyzed by means of digital image processing.

Of particular notice are the experiments by H. Fiedler at the Technische Universitat Berlin in a shear layer with favorable pressure gradients. The facility in Tucson is capable of such an adjustment, and related experiments will be explored in follow-up activities. The effect of adverse pressure gradient on the two-dimensional mixing layer may be of prime importance in the flow field associated with dynamic stall.

3. Progress Report

3.1 Development of Experimental Methods and Facilities

At the time the proposal was written, a new closed circuit water shear layer facility had just been made available to us by Professors H. Fiedler of the Technische Universitat Berlin and I.J. Wygnanski of Tel-Aviv University. The new facility was assembled in the Hydrodynamics Research Laboratory and the first test runs were conducted in November 1985. In this section we briefly describe the facility and the design changes that took place during the course of its testing and calibration. We also touch on the present status of the large suite of flow diagnostic tools that we proposed to develop and which, we believe, are essential to the successful completion of our proposed experimental investigation.

3.1.1 The Water Shear Layer Facility.

The facility is shown in Figure 1. The two streams originate from the same reservoir and are driven by a single pump powered by a 10 hp motor equipped with a solid state speed controller (VF PACK-P). The velocity of each stream and the velocity ratio can be independently varied. Test-section velocities up to 200 cm/sec can be realized. The test section and the contraction were redesigned through the course of the preliminary test runs. The test section (10 cm x 20 cm span x 100 cm long) is now equipped with a boundary-layer suction device at the inlet and four independently removable Lucite walls so that the flow may be observed from any direction. The

convergence of the test section on either side of the shear layer may be adjusted in order to vary the streamwise pressure gradient. The contraction (with a contraction ratio of 9:1) has a rectangular cross section with a constant aspect ratio. The contraction contours were formed using a fifth order polynomial. This design helps minimize the thickness of the boundary layers on the splitter plate and on all side walls. Turning vanes and "turbulence manipulators" (honeycomb and screens) upstream of the contraction help reduce velocity fluctuations due to secondary flow. The splitter plate is removable and is configured with various combinations of surface heaters.

Instrumentation includes a pressure transducer (Rosemount model 2051, 0.1% accuracy @ 2" H_2O) in conjunction with two 12 port fast switches (Scanivalve type W0601/1P-12T). These switches are computer controlled and allow for monitoring the velocity on either side of the contraction exit plane, the static pressure along the test section, and pitot-static measurements of the velocity field within the test section. The water temperature is monitored and recorded by the laboratory computer via a digital thermometer (Fluke model 2180A, 0.01 ^{o}C resolution). Eight dye injection ports are available on each side of the flow partition. A computer controlled two-axis traverse mechanism designed for detailed measurements of the flow field within the test section with rakes of either hot film probes or total pressure tubes has been installed in the facility.

3.1.2 Surface Film Heaters

Excitation of steamwise and spanwise instability modes in the shear layer is accomplished by a mosaic of surface film heaters mounted on the splitter plate. The effect of heating the surface is essentially to introduce a controlled vorticity distribution into the splitter plate boundary layer (Liepmann et al., 1982). It is important to recognize that small induced oscillations in the boundary layer amplify or decay according to linear stability theory. Thus, forcing a shear layer from an upstream boundary layer may not be effective if the induced waves decay appreciably before they reach the trailing edge. Hence the forcing frequency should be within the unstable (amplified) range of the boundary layer, the extent of which depends strongly on the pressure gradient. By

carefully extending the splitter plate into the test section we were able to tune the streamwise pressure gradient so that it became slightly adverse, thus causing the splitter plate boundary layer to become less stable, and hence more receptive to forcing.

After considerable development, we have constructed a mosaic of surface film heaters (Figure 2) consisting of 14 spanwise-uniform elements, and two spanwise rows each having 16 individual elements. The heaters are made of Inconel and are mounted on a standard epoxy board substrate. A thin film coating, selected for good heat conduction, protects the surface of the heaters from corrosion and provides electrical insulation. Each heating element is wired through the epoxy board (using through-hole plating) and the flow partition to an individual DC power amplifier. We have recently completed the construction of 32 channels of power amplifiers, each capable of continuously driving 10 A into a load of 2-4 ohms. The total power available is limited by the power supply unit to 2.5 kW. At present, 16 channels of power amplifiers are directly driven by the laboratory computer via a D/A interface. This allows the input of arbitrary temporal waveforms to the heaters without any distortion, by compensating in software for variations with temperature in the heaters' resistance and for the fact that Joulean dissipation is quadratic in input voltage.

3.1.3 Flow Diagnostics

We are currently working on the implementation of particle streak velocimetry by means of optically activated tracers, using a small scale water jet facility as our testbed. This flow was chosen for the development of this technique because its spatial structure can be well controlled and is independently documented. The flow is uniformly seeded with neutrally buoyant phosphorescent particles having a nominal diameter of 100 microns (Delitzsch and Schmidt, 1977). A nitrogen laser (Multilasers model MO-800) briefly illuminates the flow, exciting only those particles resident within the pulsed beam. The particles luminesce for a short while following excitation, during which time they also move with the flow. This creates a visible particle streak the intensity of which decays along the direction of motion. The magnitude and direction of a particle's velocity in

the plane of view can be deduced from an image of its streak which is recorded for a predetermined time interval on photographic film or by video camera. Different regions of the flow are illuminated without difficulty by moving the laser. This technique is particularly well-suited to our investigations because it does not interfere with the flow. Preliminary data analysis was performed using a Vicom digital image processing system and a video camera on loan to our department. We have recently acquired through a DOD Instrumentation Award a new Vicom VME Image Processing System based on a Sun Microsystems 3/160 computer. This stand-alone system will enable us to display, store, and process instantaneous velocity information from the flow. The system is able to conduct frame masking, averaging, integration, and convolution on the incoming data at high speeds.

In addition to the field information, detailed measurements at various points of particular interest in the flow field will be obtained by a two-component, frequency-biased laser Doppler velocimeter, the construction of which is nearing completion. Beam splitting and frequency shifting are accomplished by two partially overlapping radial phase gratings driven by hysteresis-synchronous motors (Glezer and Coles, 1982). The three watt Argon-ion laser (Lexel model 95) and its associated optics are already on hand. A three-channel digital processor was designed and fabricated to convert the raw Doppler signals into a form suitable for input to the data acqusition system.

Ten channels of hot wire/film anemometry (AA Lab Systems) are now available for simultaneous measurement of instantaneous velocity distributions. A rake of ten closely spaced (7.5 mm apart) hot wire probes, suitable for use in water, was developed (Figure 3) and mounted on the test section traverse mechanism for simultaneous cross-stream or spanwise measurements of the streamwise velocity.

A Masscomp laboratory computer system, including 16 channels of 12 bit A/D, 16 channel of D/A, and 32 channels of general-purpose I/O, is dedicated to experiment control and data processing.

The introduction of controlled vorticity distribution into the splitter plate boundary layer by the surface film heaters is accompanied by small localized density gradients in the boundary layer fluid. The corresponding gradients in index of refraction are exploited for flow visualization by means of a Schlieren system which was designed and built for this purpose. This technique allows for a nonintrusive study of the effect of forcing on the flow in planes parallel and normal to the flow span. The resulting streaklines of heated fluid particles are recorded by a video camera in a form suitable for digital image processing.

3.2 Testing and Calibration of the Water Shear-Layer Facility

As with any new facility, considerable time was spent in extensive testing, calibration, and documentation of the flow in the test section. In particular, we report here some measurements taken at U_1=34 cm/sec and U_2=20 cm/sec (velocity ratio=0.6 or $r=[U_2-U_1]/[U_2-U_1]=0.25$). The walls on either side of the shear layer were adjusted to account for the boundary layers on the internal surfaces of the test section and the entrainment into the shear layer (Dimotakis, 1986), in such a way that the freestream velocity on either side of the layer remained constant downstream of the splitter plate. The turbulence level in each stream was less than 0.15%.

The spanwise uniformity of the flow may be inferred from cross-stream profiles of mean streamwise velocity at eight equally-spaced spanwise locations (approximately 1 cm apart) which were measured at four streamwise stations and are shown in Figure 4. Of particular note is the small deficit wake in the velocity profile measured at x=5.1 cm. At x=12.7 cm, the wake component is no longer present and the velocity profile has developed the approximate shape of a hyperbolic tangent. Small spanwise variations in the streamwise velocity within the shear layer are apparent at x=20.3 cm and x=27.9 cm. The flow is turbulent at these streamwise locations and we believe that these variations indicate the appearance of streamwise vortices (Jimenez 1983).

Several cross-stream profiles of mean streamwise velocity measured at equally spaced streamwise locations (x=7.6 cm through 27.9 cm) are plotted in similarity variables in Figure 5. The

growth of the momentum thickness with distance from the trailing edge of the splitter plate is shown in Figure 6. Notice that beyond x=75 mm the shear layer is turbulent (the momentum thickness grows linearly with downstream distance). The experimentally determined vorticity thickness of the layer, defined as $\delta_\omega=\Delta U/(\partial u/\partial y)_{max}$ is plotted in Figure 7. It was also verified that a relatively long laminar flow regime can be maintained downstream of the splitter plate at the same velocity ratio simply by reducing the freestream velocity. This may be useful for our future studies of stability and transition.

A mosaic of spanwise heating elements was installed on the splitter plate to study the effect of their streamwise location and length on the flow response. These heating elements were etched on copper coated epoxy substrate in a closely spaced formation using printed circuit technology. The nominal resistance of each indivdual heater was 1.2 Ω and its streamwise length was 0.6 mm. The effective streamwise length of the heated area could be changed by activating several heaters simultaneously.

The effect of temporally-periodic, spanwise-uniform heating was measured in both the splitter plate boundary layer and the ensuing shear layer using hot film anemometry. Four adjacent surface heaters (Re_δ*=283,300,312,320) were employed. Each heater was driven at 60 watts rms, and the maximum surface temperature was approximately 20° C above the freestream water temperature. The response of the boundary layer to excitation by each of the heaters over a range of forcing frequencies was deduced from power spectra $P(\omega)$ of the streamwise velocity measured just upstream of the trailing edge of the splitter plate (Re_δ*=420). Several runs over a range of forcing frequencies ω_f were made. Figure 8 shows $P(\omega_f)$ as a function of ω_f for the upstream heater (15 cm from the trailing edge). Similar analysis of velocity data taken when the flow was excited by the downstream heaters revealed a considerable diminution in $P(\omega_f)$ over the same frequency range. We conclude that the diminished response of the flow to surface excitation results, in part, from surface roughness introduced by the heaters (the heater thickness is approximately

3.5% δ^*). This problem has been reduced considerably by coating the surface of the splitter plate with a thin polymeric film.

Two heaters (one located at the trailing edge of the splitter plate and the other 12.5 cm upstream) were used separately to assess the response of the shear layer to spanwise-uniform excitation. Several runs similar to the boundary layer study described above were made over a range of forcing frequencies. Power spectra $P(\omega)$ of the streamwise velocity were measured 6 cm downstream of the splitter plate and 1 cm above its centerline (on the high speed side) for each forcing frequency ω_f. The power spectral density at ω_f as a function of ω_f for each heater is shown in Figure 9. In addition to the relative difference in the amplitude of the flow response, one may also note that the bandwidth of the amplified frequencies is much narrower when the excitation occurs at the trailing edge of the splitter plate.

Photographs in the cross-stream plane of a mixing layer subjected to spanwise uniform excitation are shown in Figure 10. The flow is visualized by dye injected into the boundary layer of the low speed side. When the forcing frequency is equal to the natural frequency of the shear layer (Figure 10a) the spanwise vortices appear to be formed at the natural frequency and initially move downstream in an orderly fashion without amalgamation. When the forcing frequency is equal to the one half the natural frequency of the flow (Figure 10b), vortices are shed from the splitter plate at the natural frequency and immediately undergo pairing to form a larger vortex. These results are in agreement with previous observations of Ho & Huang and Roberts in low speed water facilities.

Cross-stream profiles of mean streamwise velocity of the forced flow were measured at a number of streamwise locations and are plotted in similarity co-ordinates in Figure 11. The corresponding velocity profiles of the unforced flow are also plotted for comparison. These data clearly demonstrate that the forced shear layer spreads more in the cross-stream direction than does the unforced flow. Although the velocity profiles of the forced flow appear to be self-

similar, the difference in momentum thickness ($\Delta\Theta$ in Figure 12) between the corresponding forced and unforced flows shows considerable streamwise variation. This is reminescent of the downstream evolution of momentum thickness in the experiments of Ho & Huang under similar forcing conditions.

We have recently conducted our first test runs involving steady spanwise nonuniform excitation. Streaklines of heated fluid elements were visualized in the spanwise plane and recorded on photographic film (Figure 13) by means of a Schlieren system (§3.1.3). Steady excitations having various spanwise waveforms were synthesized by a 16-element heater array (§3.1.2): a) a square wave with wavelength equal to the width of two adjacent heating elements, one of which is powered; b) a square wave with wavelength equal to the width of four heating elements, two of which are powered; c) a sinusoid with wavelength equal to the width of eight heating elements; d) same as 'c' but shifted in the spanwise direction by four heating elements. These photographs clearly illustrate the capability of our forcing technique for flow manipulation.

Although we have mentioned only a few of the steps in our testing procedure, we believe that we have convincingly demonstrated that we now have the high quality facility and instrumentation necessary for our proposed experimental investigation. We have already begun a research program on the origin and evolution of spanwise instability in a two-dimensional shear layer. In particular we would like to focus this proposal on the important aspects of pulsed two- and three-dimensional excitation of a time-periodic base flow. In the next section we outline the motivation for this work and some preliminary results.

3.3 Spatial and Temporal Evolution of a Pulsed Two-Dimensional Excitation in a Forced Turbulent Mixing Layer

The excitation of instability modes in the plane mixing layer has been accomplished to date by introducing two-dimensional sinusoidal wavetrains into the flow. Although the study of discrete instability modes, provided some insight into the evolution of the natural (unforced) flow, the

temporal evolution of disturbances could not be fully assessed. This is because the externally excited modes can only evolve in space while their temporal evolution is inhibited by the predetermined frequency of the excitation and some of its leading harmonics. The importance of the simultaneous temporal and spatial growth was established by Gaster and Grant (1975) who studied the evolution of a wave packet in a laminar boundary layer. Gaster (1987) concluded that the wave packet evolving in space and time may lead to transition much earlier than a continuous wavetrain of comparable amplitude.

In order to shed some light on the spatial and temporal evolution of the unforced plane mixing layer, we conducted an exploratory study of the development of an **isolated two-dimensional disturbance** in this flow. The disturbance was introduced into the flow by means of a momentary motion of a flap mounted at the trailing edge of the splitter plate and spanning the test section. The measurements were done in air in the facility described by Oster and Wygnanski (1982). The velocities of the respective streams were U_1=5 m/sec. and U_2=3 m/sec. The procedures of data acquisition and some of the basic processing are reported in earlier studies of Oster et al. (1982), Weisbrot (1984) and Glezer et al. (1987).

It was apparent from the outset that the irregularities in the unforced mixing layer resulted in a substantial scatter in the amplitude and arrival time of the disturbance at the location of measurement. In order to minimize this difficulty at the early stages of this research, it was decided to induce a clear phase reference in the flow by superimposing the momentary disturbance on a lower-level, two-dimensional, sinusoidal wavetrain at low duty factors. A typical signal used to activate the flap is shown in Figure 14. The period of the input disturbance was 50 [msec.] and the amplitude of the "pulse" was either three or five times higher than the amplitude of the continuous wavetrain. The background sinusoidal excitation helped to preserve the two-dimensional nature of the perturbation propagating in the flow by supressing the evolution of spanwise instabilities (Oster

et al. 1979, Metcalfe et al. 1986). In what follows, we shall briefly touch upon some of our preliminary results.

Phase locked measurements of the streamwise velocity were taken across the mixing layer at numerous streamwise locations. A typical temporal record contained between 5 and 10 cycles of the background perturbation depending on the sampling-rate of the data. Ensemble-averaged time-series representing the velocity records measured across the mixing layer at x=400 [mm.] from the splitter plate are shown in Figure 15a. The mean velocity profile in the background flow is shown on the left-hand side of this figure and although the vorticity thickness of this profile is only 24 [mm.], fluctuations in the background velocity are clearly visible at distances of 60 [mm.] above and below the center-line of this flow. The background wave appears to be sinusoidal at $|y| \geq 60$ [mm.] while it is obviously distorted at $|y|=20$mm. The momentary disturbance is felt across the entire shear layer at $T \simeq 100$ [msec.] after its intiation by the flap. One may observe that at $y \geq 40$ [mm.] (i.e., on the high velocity side of the base flow) the disturbance velocity is mostly positive, while at $y \leq -40$ [mm.] the disturbance velocity is mostly negative. Also, the duration of the disturbance on the high-speed side of the flow appears to be much longer. Reproducing these measurements at x=600 [mm.] indicates that an additional 50 [msec.] is required for the disturbance to arrive to the new x location and suggests that it is approximately convected at the average velocity of the two streams [i.e., $Uc=0.5*(U_1+U_2)$]. The amplitudes of the background waves were increased at comparative y locations and harmonic distortions can be observed in the central region of the shear layer (Figure 15b). The vorticity thickness of the mean velocity profile almost doubled in width between x=400 [mm.] and x=600 [mm.].

A quantitative description of the travelling perturbation, henceforth referred to as the "blip", can be obtained by subtracting the mean and the oscillatory background flow. It appeared to be a simple task until it was realized that the "blip" causes a shift in the phase of the background wavetrain. This effect can be demonstrated by replotting the oscillations in velocity during a single

period of the wavetrain over the entire temporal record. The dashed curve in Figure 16a represents a repetition of the data measured during the first 50 msec. of the recorded time series. As the "blip" approached, not only did deviations in amplitude become noticeable but also deviations in phase. This phase shift is not immediately restored after the passage of the perturbation, in fact it may not be restored at all as evidenced from the extended temporal record shown in Figure 16b. Consequently a **simple substraction of the oscillatory background velocity is incorrect.**

A demodulation technique [described in the Appendix] was developed in order to isolate the phase locked disturbance from the background flow. This technique is essentially a decomposition of the disturbance into a family of "modal" two-dimensional wave packets given by

$$s_i(\mathbf{x},t) = [A_i(\mathbf{x}) + C_i(\mathbf{x},t)]\ \sin[\omega_{0i}t + \phi(\mathbf{x},t)] \qquad [3.1]$$

where ω_0 is the "fundamental" frequency of the excitation and i is a summation index over its higher harmonics.

The modal decomposition enables us to study the features of the disturbance in detail, and, in particular, the propagation, amplification and some of the nonlinear aspects of its modal components. We present here some examples of the utilization of this technique. Figure 17 is a plot of a wave packet whose frequency is centered around the fundamental (i=1) frequency. The packet is plotted as a function of time at a number of streamwise locations [marked on the ordinate of Figure 17] along rays corresponding to a constant mean velocity measured in the absence of the "blip" and given by: $(U-U_1)/(U_2-U_1)$=25%; 50%; and 75%. These data indicate that the maximum amplitude of the packet diminishes with increasing x while its duration increases and thus, the overall kinetic energy in the packet might very well have increased with x. At x=500 [mm.] the kinetic energy in the "blip" attained a local minimum on the high-speed side of the central region [i.e., $y>y_{50}$] of the mixing layer [Figure 17b,c] while beyond this distance a secondary amplification seems to been taking place. The envelope of the demodulated packets is also plotted in Figure 17 to

show the change in the extent of the "blip" with increasing time and streamwise distance. One may repeat this procedure by replotting the variation in velocity with x at a given time. Although the resolution is not very good in this case [it is equivalent to a sampling rate of 166 samples/second and provides approximately 8 points/cycle at the fundamental frequency], it is adequate for the delineation of the wave packet [Figure 18].

Finding the envelope of the "blip" at a given time and integrating it over x and y represents the overall amplitude of the waves in the "blip" at a given time. The normalized, temporal evolution of the "blip" is plotted in Figure 19a. Since the square of this quantity [shown in Figure 19b] is proportional to the kinetic energy contained by the fundamental frequency, one may observe that the energy in the "blip" increases with time for T<115 [msec.] and decays thereafter. The rapid decrease in the integrated amplitude at T>120 [msec.] which is not borne out by a similar decrease in the square of this quantity reveal that some of the decrease stems from $C_i(x,t)$ being negative. The amplitude of the harmonic component of the "blip" does not increase during the amplification period of the fundamental but decreases somewhat thereafter [Figures 19a,b]. Determining the time at which the centroid of the "blip" occurs and integrating the quantity:

$$\int [A_i(x) + C_i(x,t)]\, dy \qquad [3.2]$$

or:

$$\int [A_i(x)]\, dy \qquad [3.3]$$

across the mixing layer, yields the amplification of the wavetrain plus the "blip" or the amplification of the wavetrain alone in the direction of streaming [Figure 20]. The amplification of the wavetrain with x is identical to the amplification measured by Gaster, Kit and Wygnanski (1985). The initial amplitude of the streamwise velocity perturbation at x=200 [mm.] in the centroid of the "blip" [i.e., the integral presented in equation 3.3] is 3.5 times larger than the corresponding perturbation in the wavetrain. The rate of amplification of this quantity with x, however, is larger than the

corresponding rate in the wavetrain. Saturation occurs at x=500 [mm.]. Thereafter the integrated amplitude of the "blip" plus the wavetrain remains unchanged while the amplitude of the wavetrain keeps increasing provided x<750 [mm.], implying that the perturbation amplitude in the "blip" decreases with x.

One may follow the propagation of the "blip" by plotting contours of the velocity perturbation $\{Ci(\mathbf{x},y;t)\ \sin(\omega_0 t + \phi(\mathbf{x},y))$ for the entire flow-field at regular time intervals [Figure 21a]. The "blip" can, in general, be described by contours of a positive velocity fluctuation flanked by negative lobes on both the upstream and downstream side. It appears to be convected at almost a constant velocity, and at T=120 [msec.] it stretches between x=300 [mm.] and x=750 [mm.]. A very strong depression [i.e., negative lobe] in the axial velocity component occurs quite suddenly in the center of the shear layer at T>144, which also corresponds to x>600 [mm.]. A more detailed examination of these contours between 250<x<750 [mm.] reveals that the local amplitude of the waves in the "blip" does not increase appreciably with x, the "blip" stretches, however, substantially in x and thus only between 90<T<150 [msec.] is the entire "blip" within the measuring "window" which extends between 200<x<850 [mm.]. Plotting the time dependent amplitude $C_i(x,t)$ in the same coordinates reveals that 100 to 120 [msec.] after the initiation of the "blip" a negative region of $C_i(\mathbf{x},t)$ appears in the center of the mixing layer [Figure 21b]. This region stretches in the direction of streaming with increasing time but it's trailing-edge remains at x=540 [mm.] and is not convected downstream for as long as 80 [msec.]. The existence of this region, which is marked by a relative quiescence [see Figures 17b,c] corresponding to x=500 [mm.] implies that the local amplitude of the waves in the "blip" is smaller than in the surrounding wavetrain.

The distribution across the shear layer of the amplitude $A(\mathbf{x})$ and the phase Φ in the background wavetrain [see equation 3.1 or A1-8] is plotted in Figure 22. The results of this distribution resemble the results obtained by Gaster, Kit and Wygnanski (1985) shown in Figure 7 of their manuscript. Indeed, the two parameters chosen in the two experiments are identical with

the exception of the amplitude of the flap, the displacement of which was twice as high in the present experiment resulting in $dx/d\theta$=65 vs 85 in the case reported by Gaster et al. [Figure 23a]. The lateral distribution of the mean velocity profile outside the "blip" is also identical to the profile measured by Gaster et al. [Figure 23b] and therefore, when the lateral distribution of amplitudes was compared at the appropriate Strouhal number, St_θ, then the results match perfectly. The data plotted in Figure 22 depicts the change in the lateral distribution of the amplitudes across the mixing layer at intervals of 100 [mm.]. The harmonic content of the signal at each x location is also plotted in Figure 22, revealing the increasing significance of the non-linearities with increasing x.

By pick'·g the centroid of the envelope of the "blip" in both time and y at a given x location, one may plot the amplitude distribution in the center of the "blip" as a function of y. The data presented in Figure 24 indicates that the "blip" resembles the wavetrain and can probably be described as an instability mode. Since the amplitudes associated with the "blip" are much higher than the amplitudes prevailing in the wavetrain at comparable x locations, the shape of the lateral distribution of the amplitudes within the "blip" measured at x=400 [mm.] is similar to the shape of the corresponding amplitude distribution in the wavetrain measured at x=800 [mm.]. In fact, the mean flow at the two locations mentioned might become sufficiently broad to have reached its neutral amplification state based on the linear approximation. This would also indicate that the mean flow in the mixing layer is significantly altered during the passage of the "blip". The effects of the "blip" on the mean flow can be easily discerned from the three-dimensional view showing the dependence of the velocity profile on time [Figure 25]. During the passage of the "blip", the velocity profile is generally broader but the increase in width is not uniform. Plotting the dependence of the instantaneous momentum thickness on time at a given x station indicates that the oscillations in θ can exceed 300% [!] during the passage of the "blip". The variation of θ with time at x=400 [mm.] is shown in Figure 26, in this case θ oscillates between 1 and 12 mm. during the passage of the "blip" but it only changes between 3 and 5 mm. during the periodic oscillations in the

wavetrain. The effects of the "blip" on the local velocity distribution is therefore very large and should be predicted. This is perhaps the strongest case against the simple utilization of the linear theory since the model was first used by Gaster et al.

The present experiment enables us to determine the temporal evolution of the amplitudes at a given x across the entire shear layer, during the passage of the "blip". A sequence of normalized, transverse distributions of the streamwise component of the velocity fluctuations, is drawn in Figure 27 for x=400 [mm.] at time interval of 12 [msec.]. The corresponding changes in the velocity profile are also shown on this figure at the identical time intervals. At T<36 [msec.] and T>144 [msec.] the shape of the amplitude distribution (similar to eigenfunctions of the continuous wavetrain) indicates the wave associated with the "blip" amplifies with time, however at times correspoding to 60<T<96 [msec.], the shear layer became temporarily so wide that the excited wave decayed. Since the decaying "eigenfunction" has a low relative amplitude near the inflection point [i.e., near y_{50}], one expects the absolute amplitude to decrease at those locations. This might be the reason for the region of negative $C_i(x;t)$ observed in Figure 21b.

A sequence of contour plots portraying the intensity of the velocity-fluctuations measured at regular time intervals, following the input of the momentary disturbance, are plotted in Figure 28. These data show that the disturbance, which travels in the streamwise direction, first amplifies [mostly by increasing its domain rather than absolute amplitude] and then seems to weaken and disappear around x=700 [mm]. The weakening of the turbulence level starts being noticeable around T=130 [msec.] where the lateral distribution of the RMS level resembles the distribution of vorticity associated with the main instability. Specifically, when the primary instability approaches its neutral amplification point, vorticity is being re-organized by one vortex accelerating towards the other. At the neutrally stable point, the two vortices are displaced in the lateral direction only [Wygnanski and Weisbrot 1987]. This appears to have occurred at T=144 [msec.] although the contours shown do not represent the vorticity distribution of the main instability. The RMS level of the small scale velocity

fluctuations appears to be closely tied to the large coherent structures as might easily be inferred from the contours shown in this figure. It is important to note that the high turbulence level within the disturbance, compared to the surrounding flow, probably leads to a transient increase in the mixing between the two fluids. This effect may present important concequences from the standpoint of the modification and control of mixing.

The somewhat idealized problem describing the evolution of a wave-packet was formulated by T.F. Balsa in an attempt to provide a theoretical support for the present study. The manuscript entitled: "AMPLITUDE EQUATIONS FOR WAVE PACKETS IN SLIGHTLY INHOMOGENOUS UNSTABLE FLOWS" is attached in the Appendix. Although, at this point in time, this study does not provide a direct comparison between theory and experiment because of lack of detailed computation, it may be used in the future to tie the physics of the problem with mathematical formulation.

CONCLUDING REMARKS

This work represents an extension of the "classical" studies of instability in free shear flows which emlpoyed two-dimensional harmonic excitation. We are now considering second-order interactions by superposing spanwise disturbances on the shear layer on the regular two-dimensional disturbances with which we are quite familiar. We are also modulating these disturbances in amplitude and we shall soon be modulating them in frequency. Based on our preliminary investigations, we believe that the additional degrees of freedom, available to the disturbance, fundamentally alter the evolution of the large coherent structures in the flow. Pulsed excitation, for example, enables us to differentiate between the evolution of the coherent structures in time and in space while the non-uniform excitation in the spanwise direction enables us to study the results of modal interactions. All these will not only improve our understanding of the coherent structures existing in the natural, unexcited state, but also will have important consequences on the modification and control of mixing.

APPENDIX

Time series containing 2N points and depicting the instantaneous velocity $u(\mathbf{x},t)$ sampled at a rate SR can be represented by discrete Fourier series:

$$u(\mathbf{x},t) = \frac{1}{2} \sum_{k=1}^{n-1} \left\{ B_k(\mathbf{x})\, e^{i\left[\frac{2\pi k}{T} t + \psi_k(\mathbf{x})\right]} + C.C \right\} \qquad [1]$$

where C.C. denotes a complex conjugate term Equation [1] can be rewritten by substituting the time T=2N/SR

$$u(\mathbf{x},t) = \frac{1}{2} \sum_{k=1}^{n-1} \left\{ B_k(\mathbf{x})\, e^{i\left[\frac{\pi SRk}{n} t + \psi_k(\mathbf{x})\right]} + C.C \right\} \qquad [2]$$

Defining f_0 as being at the center of the frequency window of interest established from the power spectra shown in Figure [A1-a], enables one to define a corresponding mode, M_0, as:

$$M_C = \text{Int}\left[\frac{2N\, f_0}{SR}\right] \qquad [3]$$

Filtering $u(\mathbf{x},t)$ using a band-pass filter $2\Delta M$ wide centered at f_0 reduces the time series to:

$$u'_C(\mathbf{x},t) = \frac{1}{2} \sum_{k=M_C-\Delta M}^{M_C+\Delta M} \left\{ B_k(\mathbf{x})\, e^{i\left[\frac{\pi SRk}{n} t + \psi_k(\mathbf{x})\right]} + C.C \right\} \qquad [4]$$

which is plotted and compared with the raw signal in Figure [A1-b]. Now define $u'(\mathbf{x},t)$ as a perturbation velocity of the type

$$u_c'(x,t) = \frac{1}{2}\left\{[A(x) + C(x,t)]\, e^{i\left[\frac{\pi SRM_c}{n} t + \phi_0(x)\right]} + C.C\right\} \qquad [5]$$

where $C(x,t)$ and $\phi_0(x,t)$ are the time dependent amplitude and phase of the perturbation. The dependence of C and Φ_0 on time stems from the fact that u_0' in equation [5] represents a single frequency f_0 while u_0' in equation 4 consists of numerous frequencies within the window M_0-ΔM and M_0+ΔM. Multiplying equations 4 and 5 by exp{-i[....]t} and equating them results in:

$$\frac{1}{2}\sum_{k=M_c-\Delta M}^{M_c+\Delta M}\left\{B_k(x)\, e^{i\left[\frac{\pi SRk}{n} t + \psi_k(x)\right]} + B_k(x)\, e^{i\left[\frac{\pi SR(k+M_c)}{n} t + \psi_k(x)\right]}\right\}$$

$$= \frac{1}{2}\left\{[A + C(x,t)]\, e^{i\phi_0(x,t)} + [A + C(x,t)]\, e^{-i\left[\frac{\pi SR2M_c}{n} t + \phi_0(x,t)\right]}\right\} \qquad [6]$$

Note that the complex conjugate terms on both sides of the equation contain frequencies centered around $2f_0$ as a result of the multiplication by exp{-i[...]t} and thus they can be easily filtered out leaving:

$$[A_0(x) + C(x,t)]\, e^{i\phi_0(x,t)} = \sum_{k=M_c-\Delta M}^{M_c+\Delta M} B_k(x)\, e^{i\left[\frac{\pi SR(k-M_c)}{n} t + \psi_k(x)\right]} \qquad [7]$$

Separating the real and imaginary part in equation [7] leads to :

$$A(x) + C(x,t) = \sqrt{R^2 + I^2} \qquad [8]$$

and

$$\phi(x,t) = \tan^{-1}\left(\frac{I}{R}\right) \qquad [9]$$

where

$$R = Re\left\{\sum_{k=M_c-\Delta M}^{M_c+\Delta M} B_k(x)\, e^{\frac{\pi SR(k-M_c)}{n} t + \psi_k(x)]}\right\}$$

$$= \sum_{k=M_c-\Delta M}^{M_c+\Delta M} B_k(x) \cos\left[\frac{\pi SR(k-M_c)}{n} t + \psi_k(x)\right] \qquad [10]$$

$$I = Im\left\{\sum_{k=M_c-\Delta M}^{M_c+\Delta M} B_k(x)\, e^{\frac{\pi SR(k-M_c)}{n} t + \psi_k(x)]}\right\}$$

$$= \sum_{k=M_c-\Delta M}^{M_c+\Delta M} B_k(x) \sin\left[\frac{\pi SR(k-M_c)}{n} t + \psi_k(x)\right] \qquad [11]$$

The overall, time dependent amplitude function [i.e, the left-hand side of equation 8] is shown in Figure [A1-c] while the time dependent phase given by equation [9] is plotted in Figure [A1-d]. The term $A(x)$ represents the asymptotic value of the amplitude at times which are either much earlier or much later than the appearance of the "blip" and ϕ gives the phase shift in the wavetrain as a result of the passage of the "blip". The value of $C(x,t)$ can be negative, implying that the amplitude of the disturbance superposed on the wavetrain is somewhat smaller than the amplitude of the wavetrain alone. The demodulated signal of the "blip" is depicted in Figure [A1-e] by the heavy dark line, while its envelope is marked by a light curve. The data shown in this figure were generated 400 [mm.] downstream of the splitter plate.

REFERENCES

Ashurst, W.T., Meiburg, E. (1985) "Three Dimensional Shear Layers via Vortex Dynamics", Sandia Report SAND85-8777.

Balsa, T.F. (1987) "Three-Dimensional Wave Packets and Instability Waves in Free Shear Layers and Their Receptivity", submitted to J. Fluid Mech..

Bernal, L.P., Roshko, A. (1986) "Streamwise Vortex Structure in Plane Mixing Layers", J. Fluid Mech., 170:499-525.

Delitzsch, V., Schmidt, D.W. (1977) "A Method of Flow Visualization Using Optically Activated Tracers", presented at the International Symposium of Flow Visualization, Tokyo, October.

Dimotakis, P.E. (1986) "Two-Dimensional Shear-Layer Entrainment", AIAA Journal, 24:1791-1796.

Gaster, M. (1987) Private Comunication.

Gaster, M., Kit, E., Wygnanski, I.J. (1985) "Large Scale Structures in a Forced Turbulent Mixing Layer", J. Fluid Mech., 150:23-39.

Gaster, M., Grant, I. (1975) "An Experimental Investigation of the Formation and Development of a Wave Packet in a Laminar Boundary Layer", Proc. R. Soc. Lond. A., 347:253-269

Glezer, A., Katz, Y. and Wygnanski, I.J. "On the Breakdown of the Wave Packet Trailing a Turbulent Spot in a Laminar Boundary Layer," submitted to J. Fluid Mech., 1987

Glezer, A., Coles, D. (1982) "A Two-Grating Method for Combined Beam Splitting and Frequency Shifting in a Two-Component Laser Doppler Velocimeter", Phys. Fluids, 25:2142-2146.

Jimenez, J. (1983) "A Spanwise Structure in the Plane Shear Layer", J. Fluid Mech., 132:319-336.

Lasheras, J.S., Cho, H. (1987) "Three Dimensional Instability of a Plane Free Shear Layer: An Experimental Study of the Formation and Evolution of Streamwise Vortices," submitted to J. Fluid Mech.

Lasheras, J.C., Cho, J.S., Maxworthy, T. (1986) "On the Origin and Evolution of Streamwise Vortical Structures in a Plane, Free Shear Layer", J. Fluid Mech., 172:231-258.

Liepmann, H.W., Brown, G.L., Nosenchuck, D.M. (1982) "Control of Laminar Instability Waves Using a New Technique", J. Fluid Mech., 118:187-200.

Lin, S.J., Corcos, G.M. (1984) "The Mixing Layer: Deterministic Model of a Turbulent Flow. Part III-The Effect of Plane Strain on the Dynamics of Streamwise Vortices", J. Fluid Mech., 141:139-178.

Metcalfe, R.W., Orszag, S.A., Brachet, M.E., Menon, S., Riley, J.J. (1985) "Secondary Instability of a Temporally Growing Mixing Layer," submitted to J. Fluid Mech.

Oster, D., Wygnanski, I. (1982) "The Forced Mixing Layer Between Parallel Streams", J. Fluid Mech., 123:91-130.

Pierrehumbert, R.T., Widnall, S.E. (1982) "The Two- and Three-Dimensional Instabilities of a Spatially Periodic Shear Layer", J. Fluid Mech., 114:59-82.

Roberts, F.A., Roshko, A. (1985) "Effects of Periodic Forcing on Mixing in Turbulent Shear Layers and Wakes", AIAA Shear Flow Control Conference, March 12-14, Boulder, Colorado.

Roshko, A. (1981) "The Plane Mixing Layer: Flow Visualization Results and Three-Dimensional Effects", in The Role of Coherent Structures in Modelling Turbulence and Mixing, Lecture Notes in Physics, (Jimenez, J., ed.), 136:208-217. Berlin/Heidelberg/New York: Springer.

Weisbrot, I. (1984), "A Highly Excited Turbulent Mixing Layer", M.Sc. Thesis Tel-Aviv University.

Wygnanski, I.J., Weisbrot, I. (1987) "On the Pairing Process in an Excited Plane Shear Layer", accepted for publication in J. Fluid Mech..

Wygnanski, I.J., Oster, D., Fiedler, H., Dziomba, B. (1979) "On the Perseverence of a Quasi-Two-Dimensional Eddy-Structure in a Turbulent Mixing Layer", J. Fluid Mech., 93:325-335.

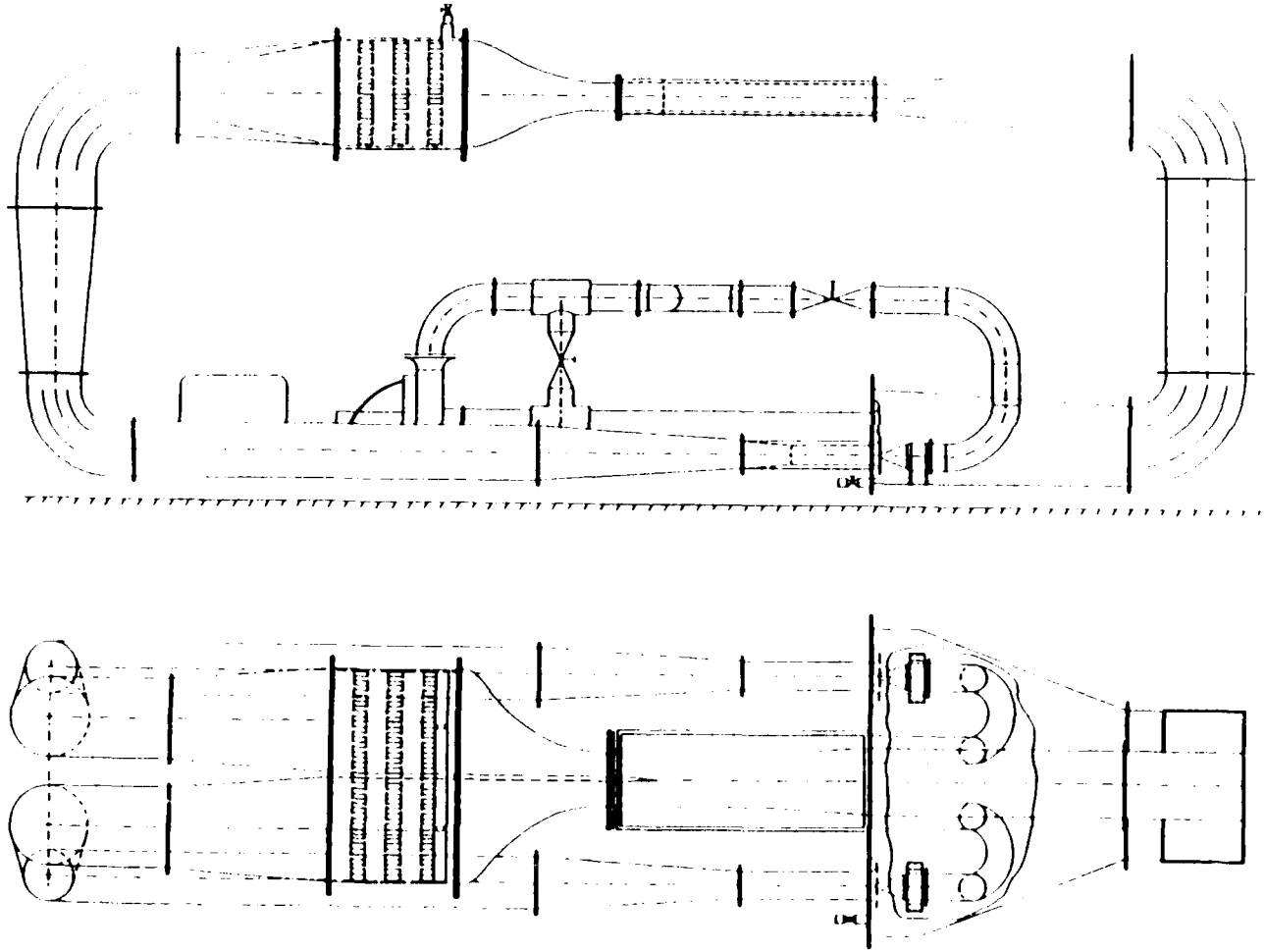

FIGURE 1

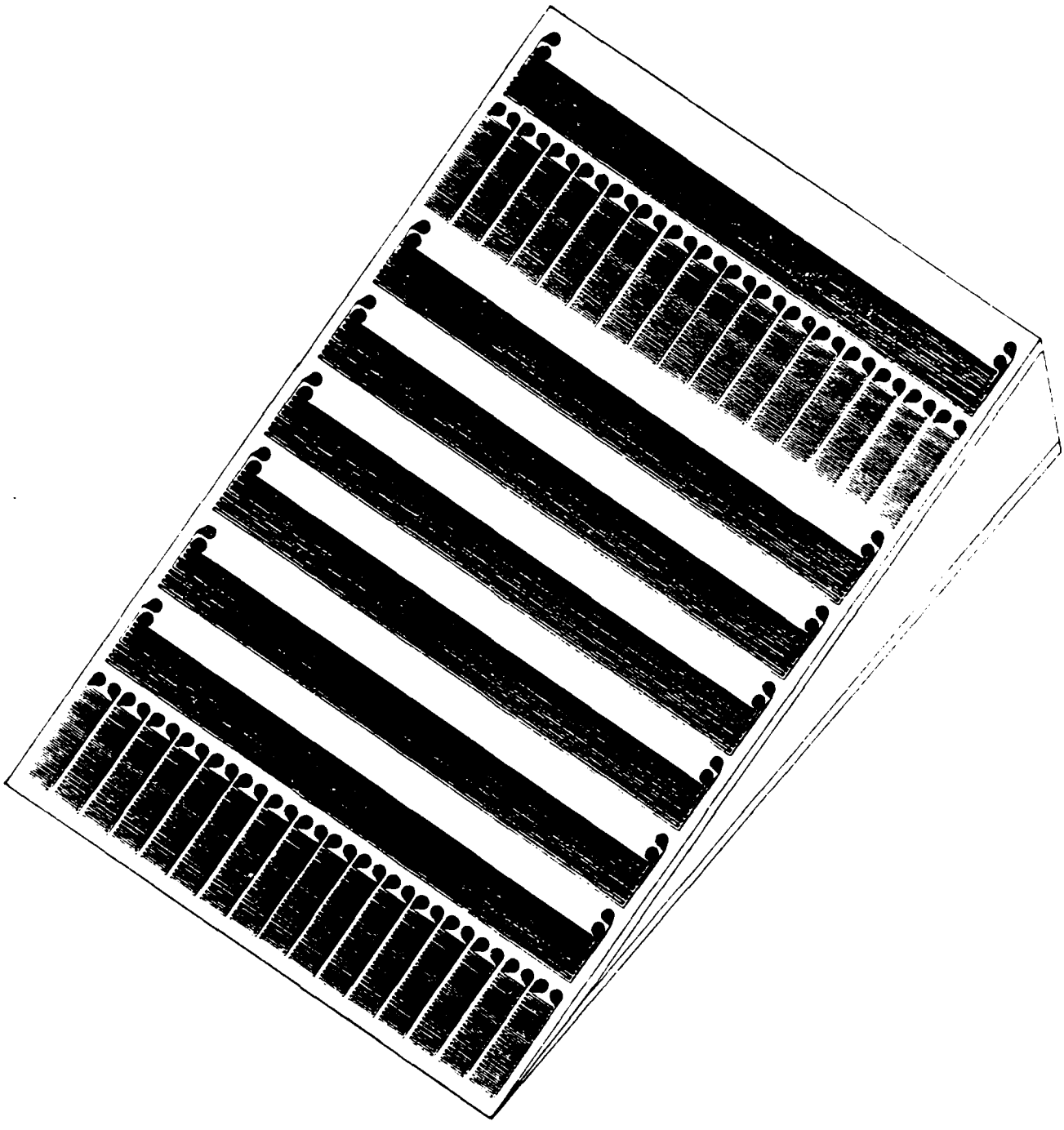

FIGURE 2

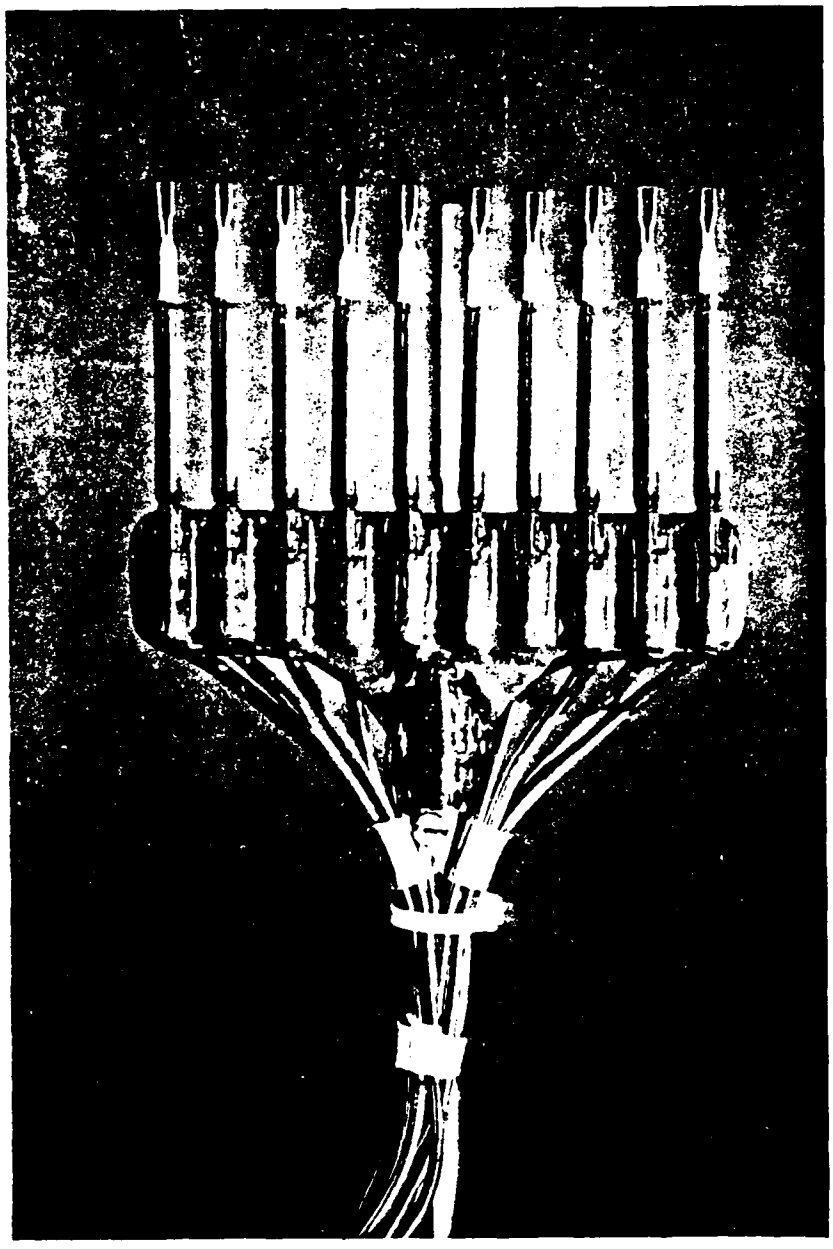

FIGURE 3

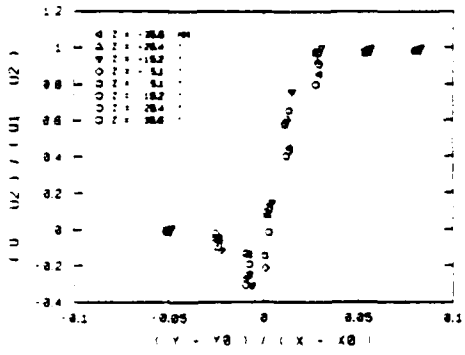

A
X=51mm

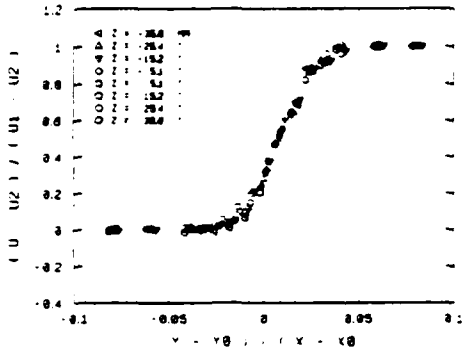

B
X=127mm

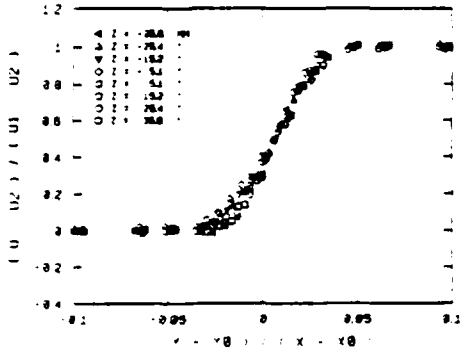

C
X=203mm

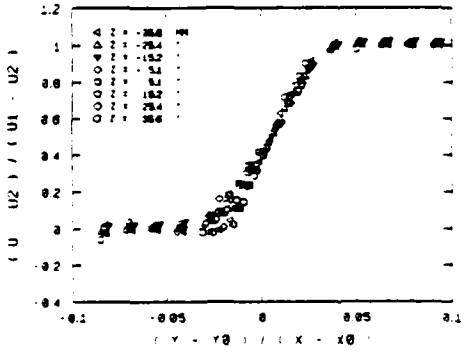

D
X=279mm

FIGURE 4

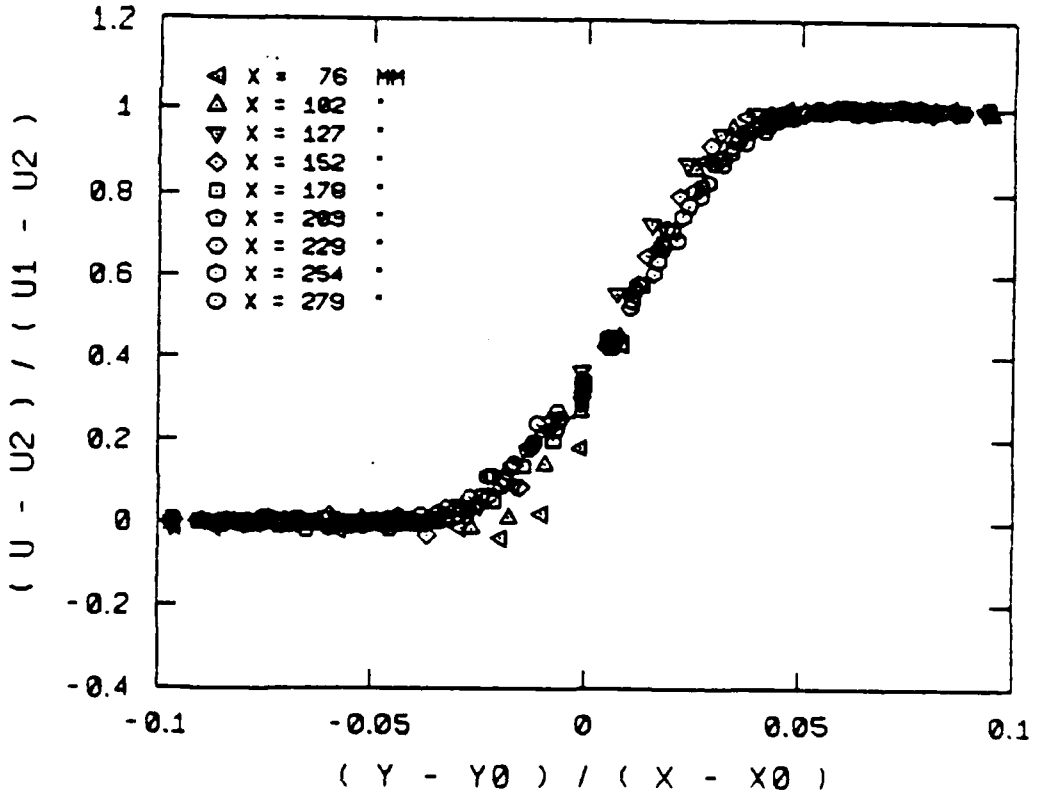
1.2
1
0.8
0.6
0.4
0.2
0
-0.2
-0.4
-0.1
-0.05
0
0.05
0.1
(U - U2) / (U1 - U2)
(Y - Y0) / (X - X0)
X = 76 MM
X = 102
X = 127
X = 152
X = 178
X = 203
X = 229
X = 254
X = 279

FIGURE 5

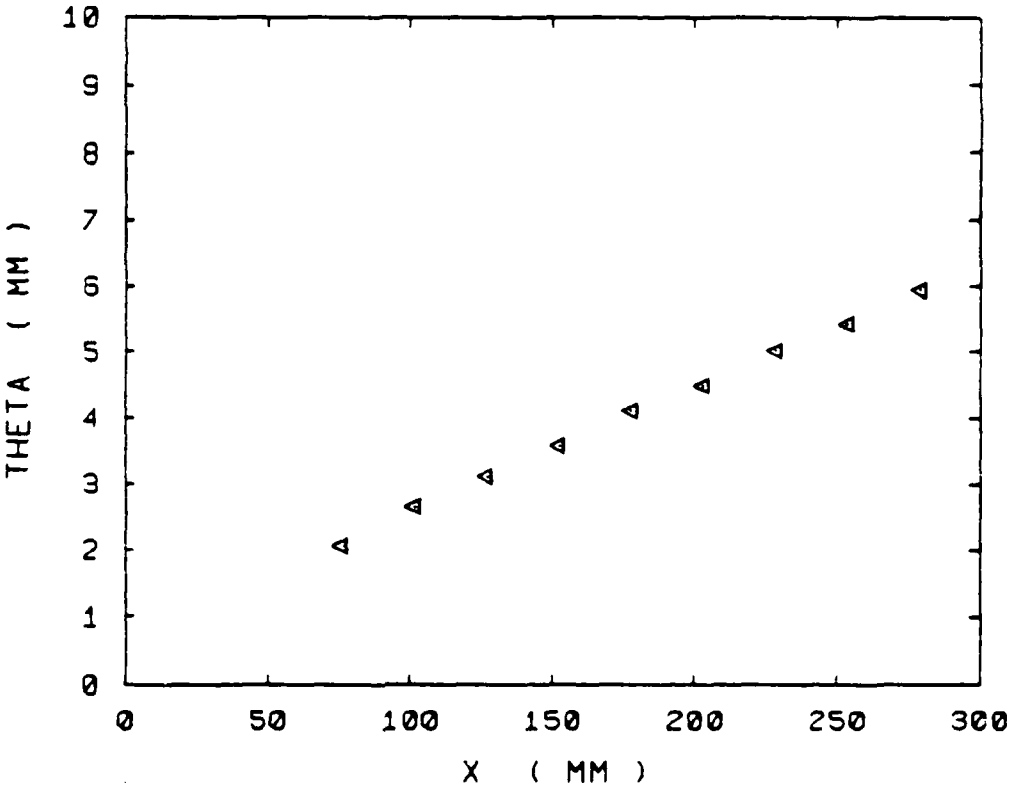

FIGURE 6

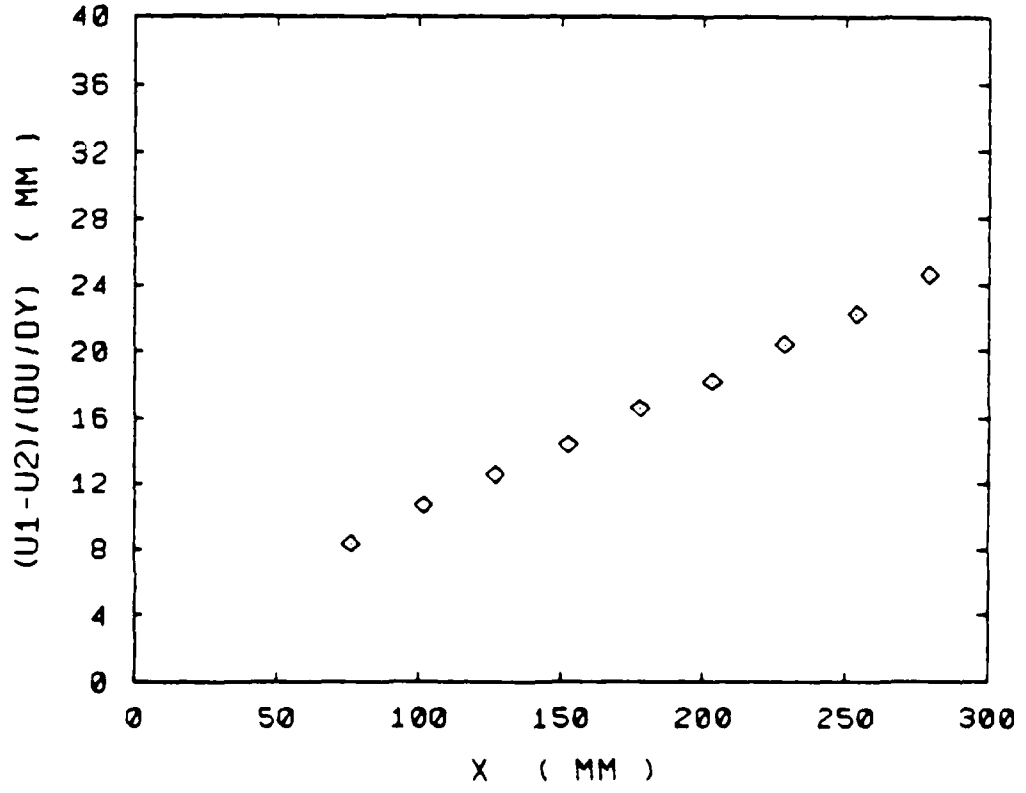

FIGURE 7

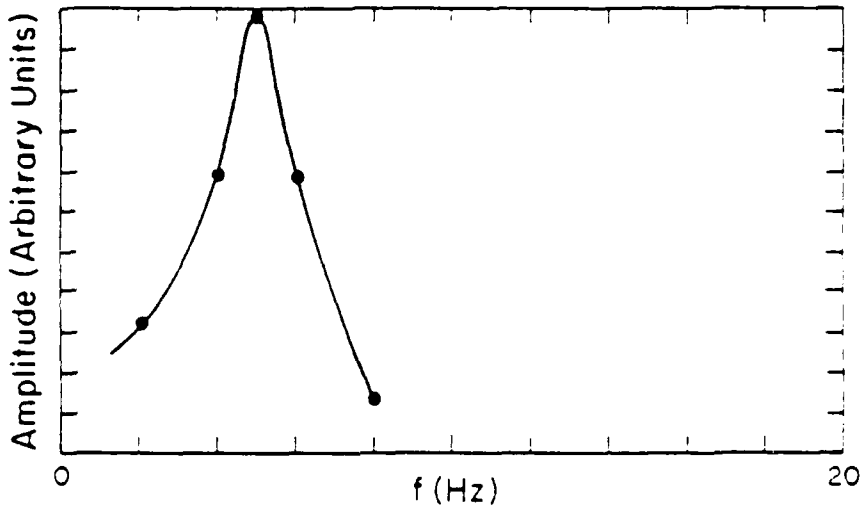

FIGURE 8

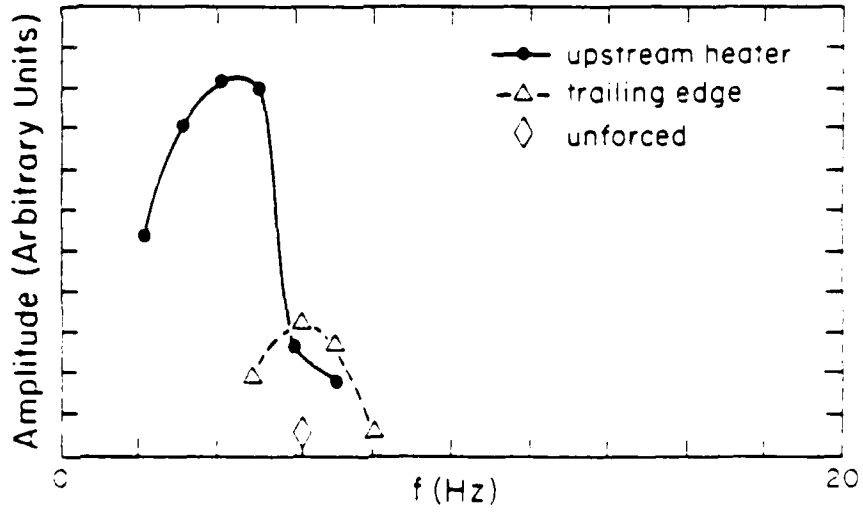

FIGURE 9

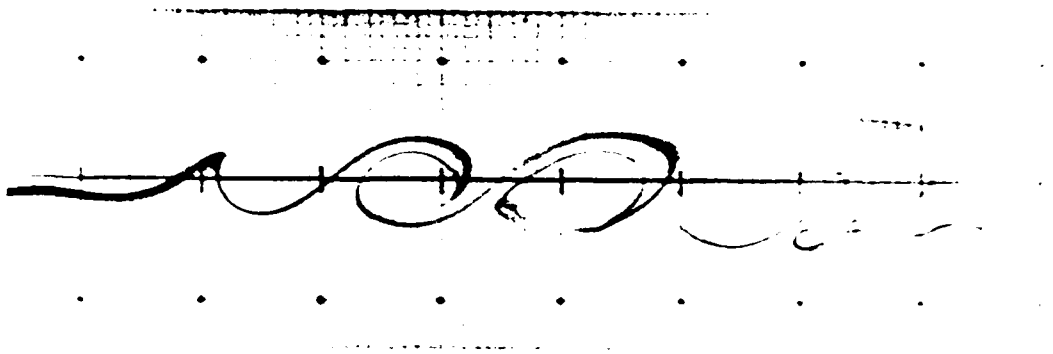

(a)

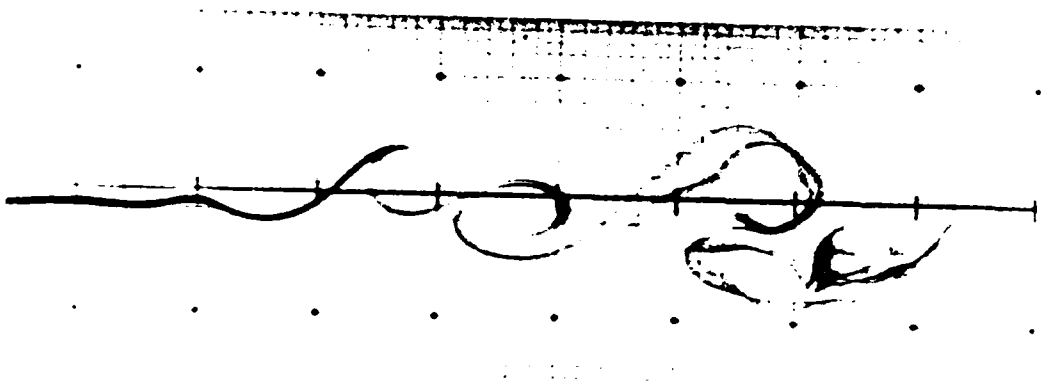

(b)

FIGURE 10

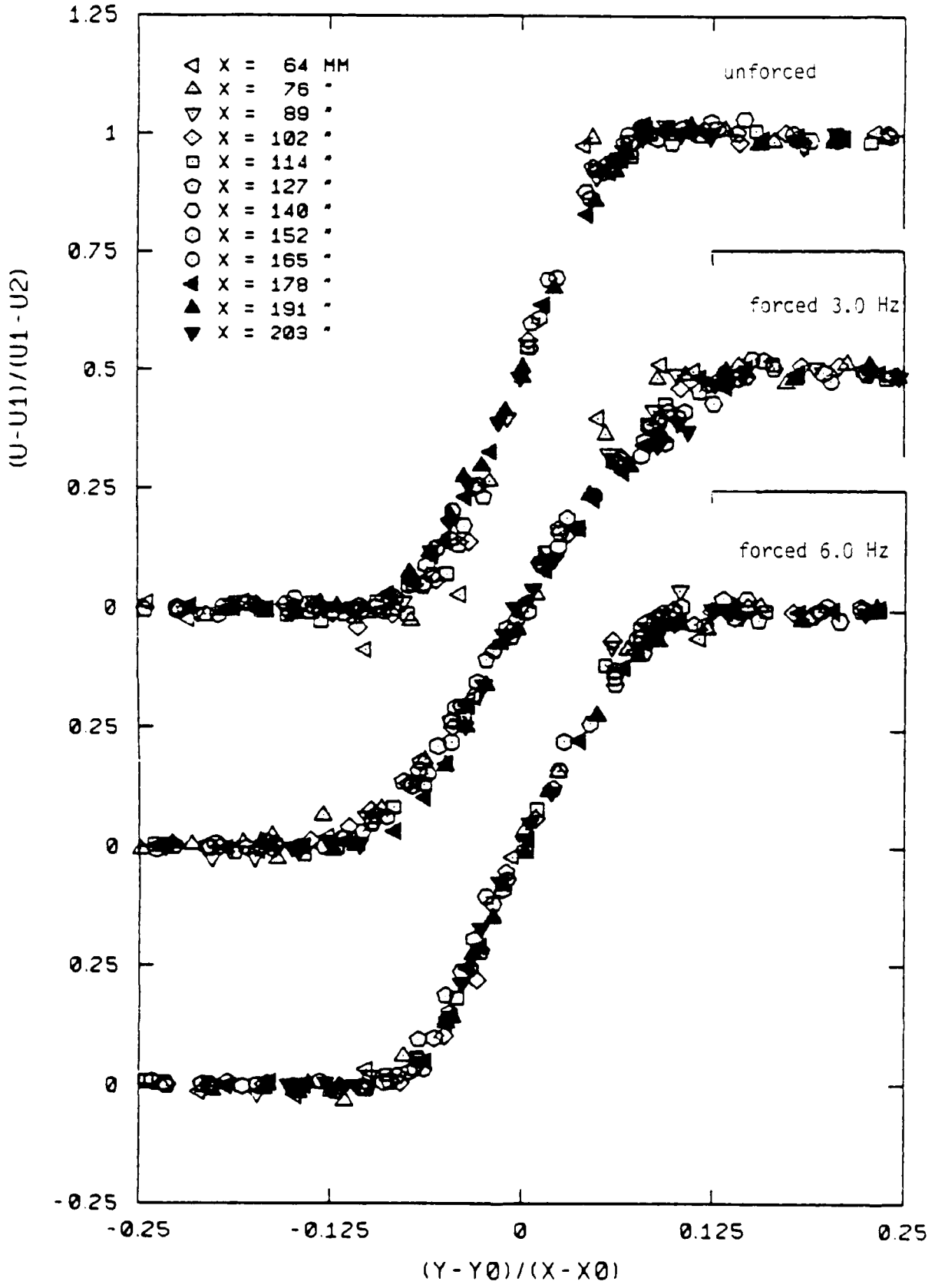
1.25
1
0.75
0.5
0.25
0
0.25
0
0.25
0
-0.25
-0.25
-0.125
0
0.125
0.25
(U-U1)/(U1-U2)
(Y-Y0)/(X-X0)
X = 64 MM
X = 76 "
X = 89 "
X = 102 "
X = 114 "
X = 127 "
X = 140 "
X = 152 "
X = 165 "
X = 178 "
X = 191 "
X = 203 "
unforced
forced 3.0 Hz
forced 6.0 Hz

FIGURE 11

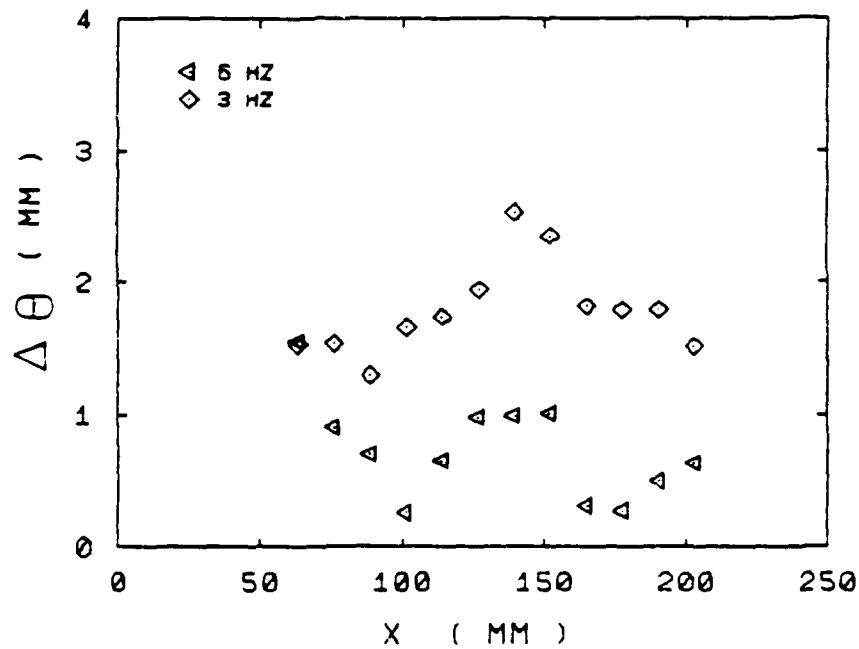

FIGURE 12

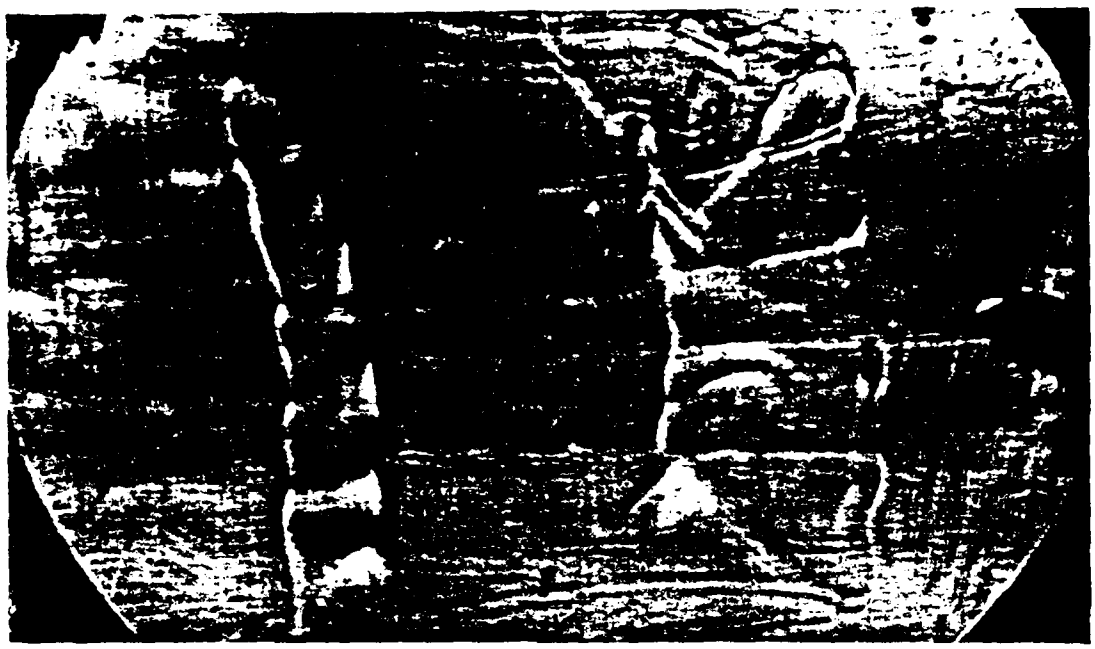

(a)

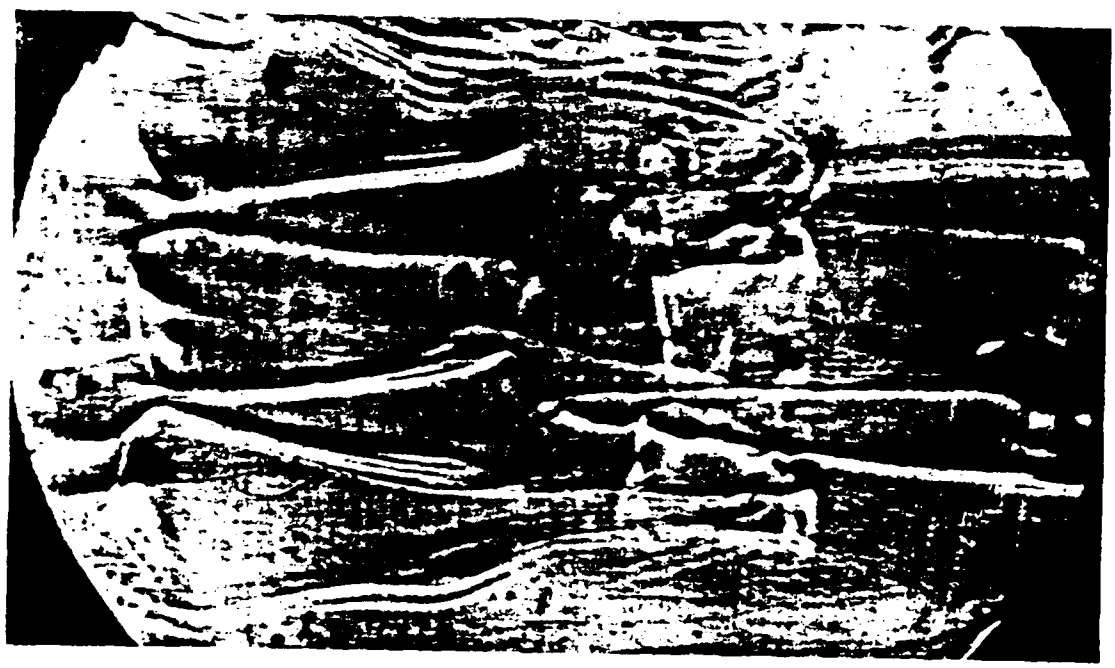

(b)

FIGURE 13

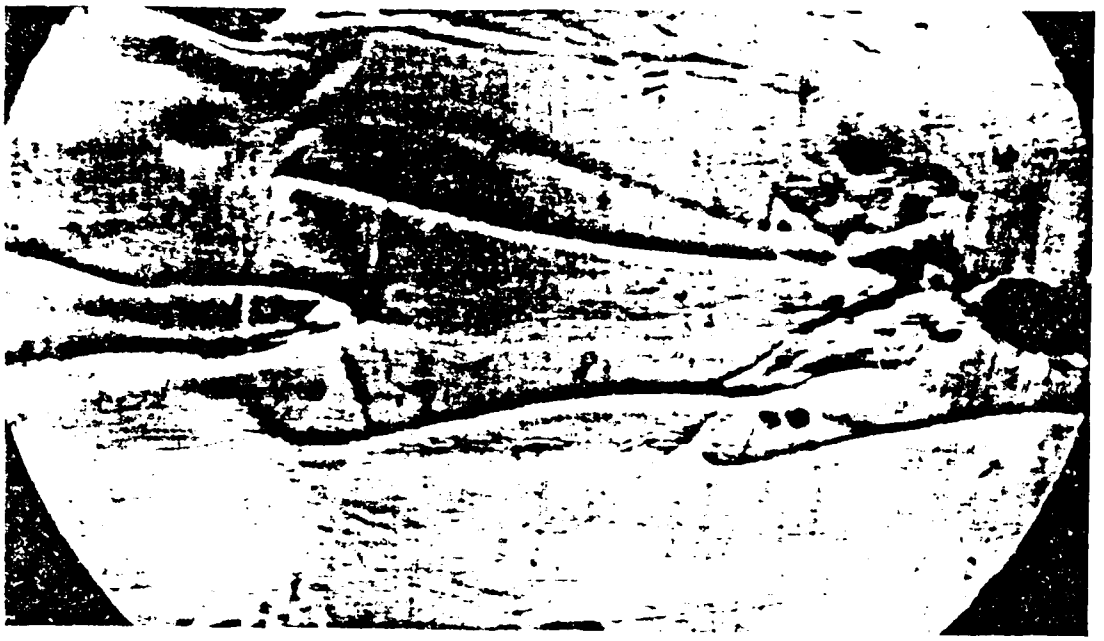

(c)

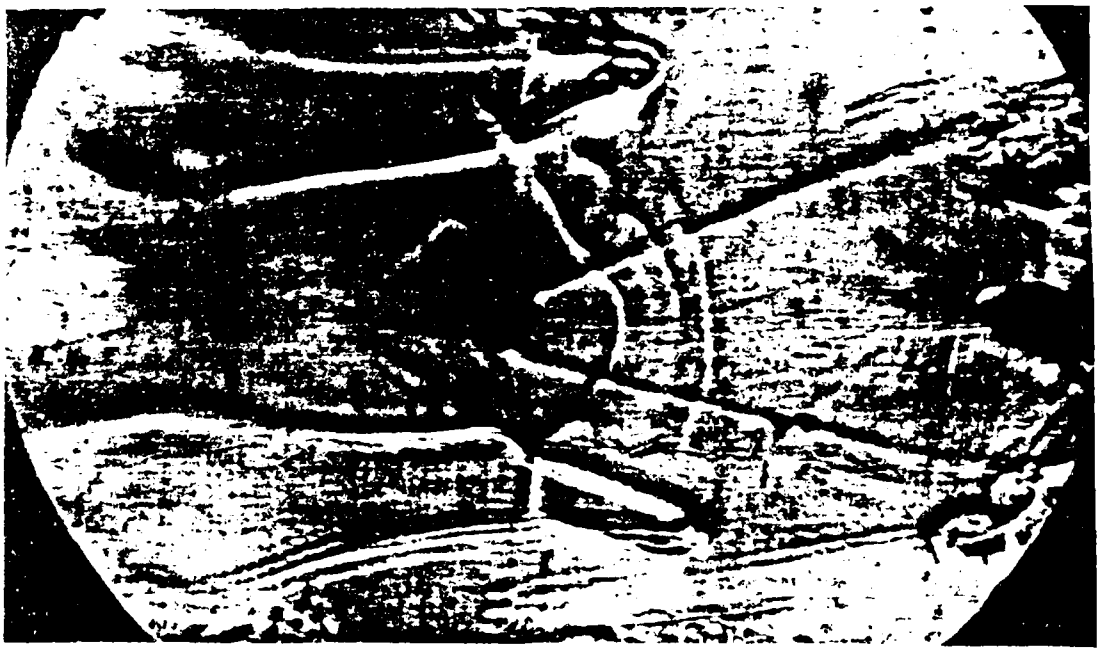

(d)

FIGURE 13

END

DATE

FILMED

5-88

DTIC